Arch. Metall. Mater., Vol. 61 (2016), No 2, p. 641–644

DOI: 10.1515/amm-2016-0109

K. GRUSZKA*, M. NABIAŁEK*, M. SZOTA**, K. BLOCH*,#, J. GONDRO*, P. PIETRUSIEWICZ*, A.V. SANDU***, A.M. MUSTAFA AL BAKRI****, S. WALTERS*****, K. WALTERS, S. GARUS*, M. DOŚPIAŁ*, J. MIZERA******

ANALYSIS OF THE THERMAL AND MAGNETIC PROPERTIES OF AMORPHOUS $Fe_{61}Co_{10}Zr_{2.5}Hf_{2.5}Me_2W_2B_{20}$ (WHERE Me = Mo, Nb, Ni OR Y) RIBBONS

The paper presents the results of structural and magnetic properties and thermal stability for a group of functional materials based on $Fe_{61}Co_{10}Zr_{2.5}Hf_{2.5}Me_2W_2B_{20}$ (where Me = Mo, Nb, Ni or Y). Samples were obtained in the form of ribbons using melt-spinning method. The X-ray diffraction patterns of investigated samples confirmed their amorphous structure. Based on the analysis of DSC curves characteristic temperatures: glass forming temperature (T_g), crystallization temperature (T_x) and temperature range of the supercooled liquid ΔT_x were determined. Small addition of transition metals elements has strong influence on magnetic and thermal parameters of studied materials. The comprehensive studies revealed that in terms of magnetic properties the Ni-addition resulted in highest reduction in coercivity and anisotropy field.

1. Introduction

History of amorphous metallic alloys despite the passage of dozens of years is still alive [1-5], because new amorphous alloys constantly are being discovered and their structure is not fully known and resolved as for crystalline alloys. In the middle of the last century, new properties of amorphous alloys were discovered. It was found, which was then completely incomprehensible that amorphous materials have domain structure and may be a magnetic material exhibiting soft magnetic properties. This fact was amazing for magnetic phenomena researchers because the domain structure was connected only with crystalline materials [6]. Then many methods for producing amorphous materials were developed, but only one method involving the solidification of liquid metal on a copper roll running at a high linear velocity was considered. The product of this process was a sample in the form of thin strips. This technique was quickly adopted by the industry. From the moment when mass production of amorphous ribbons started, groving interest in those materials emerged directed to applications. Ribbons produced using above method achieve a thickness of about 100 μm [7, 8]. It should be emphasized that these materials have unique properties compared to commercially used metal FeSi plates. It is precisely why they have been widely used in the electrical industry and the interest in them is still at a high level. In the electrical industry amorphous alloys are typically used to build low lose and almost non-magnestostrictive magnetic cores. For this type of application thermal stability of these materials is also important, because of their metastable character. It was observed that slight changes in the chemical composition of the alloys are of great importance in terms of their final properties [9]. It is therefore interesting for cognitive reasons to compare the magnetic properties and thermal stability of amorphous materials with similar chemical compositions.

The paper presents the results obtained for amorphous alloy samples with composition $Fe_{61}Co_{10}Zr_{2.5}Hf_{2.5}Me_2W_2B_{20}$ (Me = Mo, Nb, Ni lub Y) in the form of ribbons.

2. Experimental

Alloys for investigation were made with components having high purity: Fe, Co, Y, Ni, Nb, Mo = 99,98%, borium was added in the form of FeB alloy. Ingots for casting of ribbons were made in an arc furnace in an inert gas atmosphere. The solidified alloy components were melted several times to ensure good homogenization of the material. Thus prepared materials were mechanically polished and cleaned by ultrasound. Then they were divided into smaller batch portions. Alloy strips were manufactured by rapid solidification of the liquid alloy on a rotating copper roll. The liquid melt was injected under argon pressure on rotating at high speed copper wheel, an then solidified in the form of a tape.

X-ray diffraction for the investigated strips was made using BRUKER X-ray diffractometer model D8 ADVANCED. The instrument worked in Bragg-Brentano geometry and was equipped with X-ray tube with CuK_α characteristic radiation.

* CZESTOCHOWA UNIVERSITY OF TECHNOLOGY, INSTITUTE OF PHYSICS, 19 ARMII KRAJOWEJ AV., 42-200 CZESTOCHOWA, POLAND

** CZESTOCHOWA UNIVERSITY OF TECHNOLOGY, INSTITUTE OD MATERIALS SCIENCE AND ENGINEERING, 19 ARMII KRAJOWEJ AV., 42-200 CZESTOCHOWA, POLAND

*** GHEORGHE ASACHI" TECHNICAL UNIVERSITY OF IAŞI, FACULTY OF MATERIALS SCIENCE AND ENGINEERING, BLVD. D. MANGERON 71, 700050, IASI, ROMANIA

**** UNIVERSITI MALAYSIA PERLIS (UNIMAP), SCHOOL SOF MATERIALE ENGINEERING, KOMPLEKS PENGAJIAN JEJAWI 2, 02600 ARAU, PERLIS, MALAYSIA

***** UNIVERSITY OF BRIGHTON, SCHOOL OF COMPUTING, ENGINEERING AND MATHEMATICS, LEWES ROAD, BRIGHTON BN2 4GJ, UNITED KINGDOM

****** WARSAW UNIVERSITY OF TECHNOLOGY, FACULTY OF MATERIALS SCIENCE AND ENGINEERING141 WOLOSKA STR., 02-507 WARSZAWA, POLAND

Corresponding author: 23kasia1@wp.pl

The measurements were carried out through an 2θ angle range from 30° to 100° with step 0,2° and expousure time 5 s. Measurements of heat flow versus temperature was carried out by using differential scanning calorimetry (DSC). The samples were heated in the temperature range from room temperature to the liquidus temperature of approximately 1500K with constant heating rate 10K/min. DSC studies were done under Ar atmosphere. Magnetic studies were conducted using a vibrating magnetometer by "LakeShore" company working in a magnetic field up to 2 T.

3. Results and discussion

Figure 1 presents X-ray diffraction patterns obtained for the investigated samples in the form of thin ribbons.

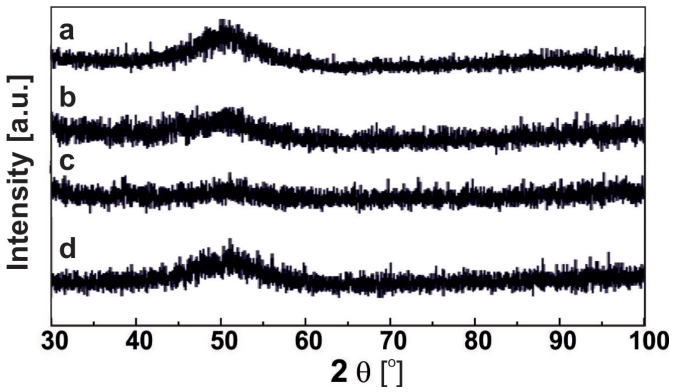

Fig. 1. X-ray diffraction patterns for the ribbon-form samples of the investigated alloys $Fe_{61}Co_{10}Zr_{2.5}Hf_{2.5}Me_2W_2B_{20}$ where Me = a) Mo, b) Nb, c) Ni, d) Y.

Designation a, b, c and d (fig. 1) represents respectively $Fe_{61}Co_{10}Zr_{2.}5Hf_{2.}5Nb_2W_2B_{20}$, $Fe_{61}Co_{10}Zr_{2.5}Hf_{2.5}Ni_2W_2B_{20}$, $Fe_{61}Co_{10}Zr_{2.5}Hf_{2.5}Mo_2W_2B_{20}$, $Fe_{61}Co_{10}Zr_{2.5}Hf_{2.5}Y_2W_2B_{20}$ samples in the state after solidification. Based on the analysis of diffraction patterns it can be concluded that they are characteristic for the amorphous materials [10-12]. For all the X-ray diffraction patterns only a single broad fuzzy maximum occurs, the top of which is located near the angle of 51 degrees. No intensive narrow peaks in the resulting diffraction patterns shows that in the volume of the materials there are no areas with long range order, determining the crystalline systems. In the amorphous materials based on FaCoB matrix it is possible to determine the glass transition temperature (T_g), which is determined as the first inflection on the DSC curve in the vicinity of the crystallization temperature (T_x). Heat flow curves as a function of temperature was measured at a heating velocity of 10 K/min in the temperature range from 300 K to 1500 K. For samples containing Nb, Ni and Y value of the enthalpy is close, and the smallest value was obtained for samples with the addition of Mo. Exothermic minimas determine the value of the energy that is needed to crystallization process to occure: Mo = 39,24 [J/g], Nb = 58,4 [J/g], Ni = 61,21 [J/g], Y = 62,52 [J/g]. All investigated alloys crystallized in a single step by a primary crystallization. Upon acquiring the appropriate free energy of the system there is a process of crystallization whose product is αFe crystalline phase. This means that in a alloy volume rearrangement of its constituents occurs and there is a separation of the Fe from amorphous matrix. Therefore, after after long range diffusion processes material consists of two phases with different chemical compositions. The difference in temperature at the beginning of crystallization (T_x) and the glass transition temperature (T_g) is called a supercooled liquid range [13-17] and is an indirect measure of the glass forming ability. Fig. 2 shows a relationship diagram T_x, T_g and ΔT_x from alloying addition Me = Mo, Nb, Ni or Y.

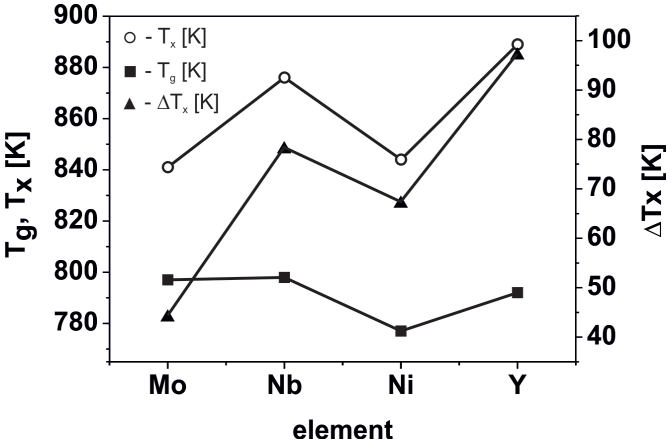

Fig. 2. T_x, T_g and ΔT_x relationship diagram vs. alloying element Me = Mo, Nb, Ni or Y for investigated samples of $Fe_{61}Co_{10}Zr_{2.5}Hf_{2.5}Me_2W_2B_{20}$ alloy.

Data obtained from the analysis of DSC curves are presented in Table 1.

TABLE 1

Tg - the glass transition temperature, Tx - crystallization onset temperature, DTx - supercooled liquid range.

Composition	T_g [K]	T_x [K]	ΔT_x[K]
$Fe_{61}Co_{10}Zr_{2.5}Hf_{2.5}Mo_2W_2B_{20}$	797	841	44
$Fe_{61}Co_{10}Zr_{2.5}Hf_{2.5}Nb_2W_2B_{20}$	788	876	78
$Fe_{61}Co_{10}Zr_{2.5}Hf_{2.5}Ni_2W_2B_{20}$	777	844	67
$Fe_{61}Co_{10}Zr_{2.5}Hf_{2.5}Y_2W_2B_{20}$	792	889	97

In the case of amorphous alloys very important parameters are those which enable to describe the determination of ability to glass transition. The thermal stability of amorphous alloys is determined on the basis of the reduced glass transition temperature ($T_{rg} = T_g/T_m$ [18]), the modified parameter of ability to form glassy state (GFA) $\gamma = T_x/(T_g + T_l)$ [18]. Parameters T_{rg}, γ, δ, temperaturre T_m i T_l are summarized in table 2.

TABLE 2

Parameters Trg, γ, and temperature Tm i Tl

Composition	T_m [K]	T_l [K]	T_{rg}	γ
$Fe_{61}Co_{10}Zr_{2.5}Hf_{2.5}Mo_2W_2B_{20}$	1319	1458	0.60	0.37
$Fe_{61}Co_{10}Zr_{2.5}Hf_{2.5}Nb_2W_2B_{20}$	1311	1454	0.60	0.39
$Fe_{61}Co_{10}Zr_{2.5}Hf_{2.5}Ni_2W_2B_{20}$	1321	1499	0.59	0.37
$Fe_{61}Co_{10}Zr_{2.5}Hf_{2.5}Y_2W_2B_{20}$	1341	1468	0.59	0.39

As stated by Turnbull [19] reduced glass transition temperature should be set to $T_{rg} \geq 2/3$. When this value is

smaller the viscosity of the material decreases, which allows diffusion of atoms at greater distances and homogeneous nucleation is more likely. For investigated alloys T_{rg} was small in range 0.50-0.60. Despite such a low value of T_{rg} each of the alloys can be prepared in an amorphous state. It was found that the change in crystallization temperature T_x and the glass transition temperature T_g for the investigated alloys are not linked to the value of the effective magnetic anisotropy field. It is known that Mo is added to the magnetic material to reduce their Curie temperature [20]. Unfortunately, a side effect of this treatment is also a lowering of the maximum magnetic polarity. In the case of alloys containing Nb, Ni, and Y compound glass transition and crystallization temperature relation with magnetic polarization saturation and the value of coercive field was observed. On this basis can be concluded that the magnetic interaction between the local magnetic moments for the investigated alloys in the form of ribbons with additives Me = Nb, Ni and Y have a significant impact on the glass transition and crystallization temperature.

The value of magnetization saturation is associated with the basic properties of the elements used as an Me additive. With increasing amount of unpaired electron located on valence shells magnetization saturation decreases. Mo, Nb, Ni and B additions have respectively 6, 5, 2 and 1 unpaired electron, and the magnetic polarization in the same statement is: 1.10, 1.12, 1.31 oraz 1.19 T. For magnetic properties are mostly responsible unpaired electrons that do not participate in interatomic bonding. It may also mean that the distribution of the Me addition in the alloy volume is not uniform which may explain the slight disturbance observed depending on the saturation magnetization of the samples with the addition of yttrium and nickel. Fig. 3 shows a diagram of Curie temperature and magnetization saturation depending on the alloy addition Me = Mo, Nb, Ni or Y for $Fe_{61}Co_{10}Zr_{2.5}Hf_{2.5}Me2W_2B_{20}$ alloys.

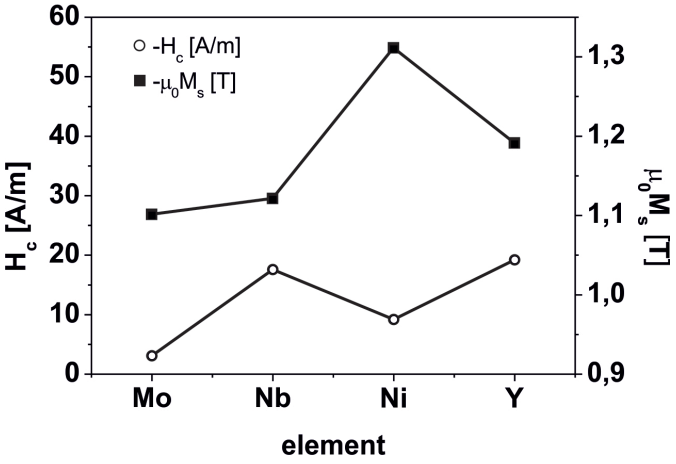

Fig. 3. M_S and H_c dependency diagram in respect of Me = Mo, Nb, Ni or Y addition in $Fe_{61}Co_{10}Zr_{2.5}Hf_{2.5}Me_2W_2B_{20}$

Data obtained from analysis of the magnetic measurements are summarized in Table 3.

An important parameter given in Table 3 describing the magnetic materials is their effective anisotropy, which in the case of crystalline materials consist of magnetoelastic and induced anisotropy [21]. Magnetoelastic anisotropy is associated with various types of stresses that are contributing to the effective anisotropy as a result of the existence of magnetoelastic feedback. In contrast induced anisotropy for the investigated alloys is the result of their manufacturing process. For the amorphous ribbons there can be distinguished mainly uniaxial anisotropy, then easy magnetization axis coincides with the direction of the magnetic field, which is also associated with the sample geometry and its shape anisotropy. Fig. 4 shows a diagram describing the dependence of the effective anisotropy for the investigated materials on the addition Me = Mo, Nb, Ni or Y.

TABLE 3.
Data from the analysis of the static hysteresis loops (VSM)

	$\mu_0 M_S$ [T]	H_c [A/m]	K_{eff} [kJ/m^3]
$Fe_{61}Co_{10}Zr_{2.5}Hf_{2.5}Mo_2W_2B_{20}$	1.10(2)	3.1(3)	88(6)
$Fe_{61}Co_{10}Zr_{2.5}Hf_{2.5}Nb_2W_2B_{20}$	1.12(2)	17.6(3)	34(6)
$Fe_{61}Co_{10}Zr_{2.5}Hf_{2.5}Ni_2W_2B_{20}$	1.31(2)	9.2(3)	26(5)
$Fe_{61}Co_{10}Zr_{2.5}Hf_{2.5}Y_2W_2B_{20}$	1.19(2)	19.2(3)	52(5)

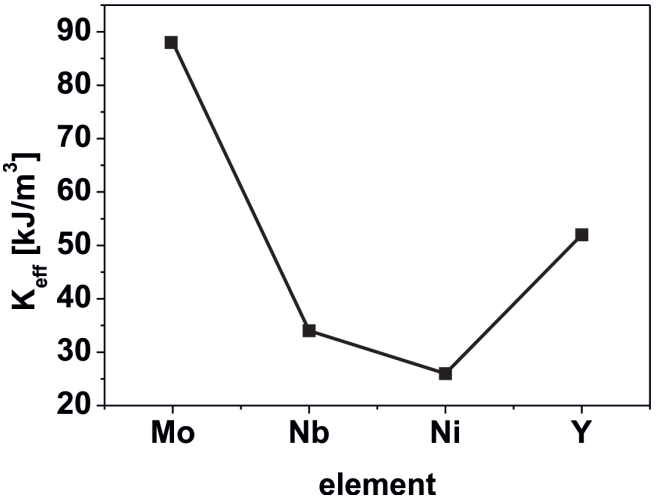

Fig. 4. Diagram describing the effective anisotropy field and the effective anisotropy energy

Samples with the addition of Mo and Y have substantially greater anisotropy field than the other two. The addition of Nb and Ni decreased significantly effective anisotropy value. The lowest effective anisotropy showed a sample with the addition of Ni, for which the lowest coercivity field and the highest saturation magnetization value was observed. The effective anisotropy field is related to the magnetic homogeneity of the sample. The lower the effective anisotropy field the higher order arrangement of the magnetic moments per unit volume, which may be associated with a decrease in the intensity of the magnetic field required for remagnetization of the material and an increase in saturation magnetization.

4. Conclusion

The melt-spinning method as indicated by the results of X-ray difraction (Fig. 1) makes it possible to produce amorphous alloy ribbons of composition $Fe_{61}Co_{10}Zr_{2.5}Hf_{2.5}Me_2W_2B_{20}$ (where Me = Mo, Nb, Ni or Y). The thermal stability of the

investigated materials is dependent on the addition of Me. Change in T_g i T_x temperatures are not related to the magnetic properties. The greatest stability of the glassy state, taking into account the width of the range of the supercooled liquid was characterized by a sample containing Y. The deterioration of soft magnetic properties and increase in the effective anisotropy field was observed after the introduction of Mo alloy element (lowering the saturation magnetization). However, this alloy has the smallest value of coercive field. Molybdenum is disturbing the magnetic structure of ferromagnetic alloy, which is connected directly with the largest number of unpaired electrons in the valence shells. Therefore, it was expected that the sample of this alloy will exhibit the most effective anisotropy field, as indicated in section Results and discussion. Effective anisotropy as described above is the sum of several components. The most important component in this case is induced anisotropy, which is directly related to the magnetoelastic anisotropy. The induced anisotropy is an effect of the manufacturing process and the rate of diffusion of atoms while achieving the glass transition temperature for the three times higher viscosity. In this stage regions of variable density and composition are formed, defining a crystallization front after delivery of additional energy. The authors expected the best magnetic properties, ie. soft magnetic properties for sample containing Nb, which is commonly used as a nanocrystalization engine. It was expected that in the volume of the alloy there are produced arrangements similar to crystalline seeds that will impact strongly reducing the value of coercive field. Of course it would not be crystalline grains but atom conglomerates characterized by smaller amount of free relaxators than in the rest of sample volume. Such assumptions were determined on the basis of the diagram included in the beginning of which is specified for the lack of crystal growth. Unfortunately, the accuracy of this diagram should be determined in two-phase systems consisting of crystalline and amorphous part on the assumption that crystal grains are of nano dimensions .

Surprisingly we obtained good performance from a sample with Y. This addition is rarely used in amorphous alloys for applications in electrical engineering. Therefore, in the design of materials for use in electric and other industries one should do the unconventional abnormal attempts, the effect of which may surprise, as in this case. In conclusion, amorphous ferromagnetic ribbons of soft magnetic properties were investigated. It was found that the parameters of the magnetic tapes may considerably vary after the minimal changes in the chemical composition of the starting alloy. As a good additional alloying element affecting mainly the decrease of the coercive field and the effective anisotropy field Ni can be successfully.

REFERENCES

[1] A.P. Thomas , M.R.J. Gibbs, J. Magn. Magn. Mater. **103**, 97-110 (1992).

[2] M. Hasiak, K. Sobczyk, J. Zbroszczyk, W. Ciurzyńska, J. Olszewski, M. Nabiałek, J. Kaleta, J. Świerczek, A. Łukiewska, IEEE Trans. Magn. **11**, 3879-3882 (2008).

[3] K. Sobczyk, J. Świerczek, J, Gondro, J. Zbroszczyk, W. Ciurzyńska, J. Olszewski, P. Brągiel, A. Łukiewska, J. Rzącki, M. Nabiałek, J.Magn. Magn. Mater. **324**, 540-549 (2012).

[4] A. Brand, Nucl. Instrum. Methods: Phys. Res. **B28**, 398 – 416 (1987).

[5] P. Pawlik, M. Nabiałek, E. Żak, J. Zbroszczyk, J. J. Wysłocki, J. Olszewski, K. Pawlik, Arch. Mat. Sci. **177**, 25/3 (2004).

[6] Z.P. Lu, C.T. Liu, J.R. Thompson, W.D. Porter, Rev. Letter. **92**, (245503-1)-(245503-4) (2004).

[7] A. Inoue, Mat. Sci. Eng. **A226-228**, 357-363 (1997).

[8] M. Nabiałek, P. Pietrusiewicz, K. Błoch, J. All. Compd., **628**, 424–428 (2015).

[9] K. Błoch, M. Nabiałek, M. Dośpiał, S. Garus, Arch. Metall. Mater., **60**, 7-10 (2015).

[10] R. Meyer, H. Kronmüller, Phys. Stat. Sol. B, **109** 693-703 (1982).

[11] M. Dospial, J. Olszewski, M. Nabialek, P. Pietrusiewicz, T. Kaczmarzyk, Nukleonika **60**, 15-18 (2015).

[12] K. Gruszka, M. Nabiałek, K. Błoch S. Walters, Int J Mater Res. **106**, 7, 689-696 (2015).

[13] M. Nabiałek, J. Zbroszczyk, W. Ciurzyńska, J. Olszewski, S. Lesz, P. Brągiel, J. Gondro, K. Sobczyk, A. Łukiewska, J. Świerczek, P. Pietrusiewicz, Arch. Metall. Mater **55**, 195-203 (2010).

[14] R. Li, S. Kumar, S. Ram, M. Stoica, S. Roth, J. Eckert, J. Phys. Appl. Phys. **42**, 085006 (2009).

[15] W.M. Wang, A. Gebert, S. Roth, U. Kuehn, L. Schultz, J. Alloys Compd. **459**, 203-208 (2008).

[16] A. Makino, T. Kubota, Ch. Chang, M. Makabe, A. Inoue, J. Magn. Magn. Mater **320**, 2499-2503 (2008).

[17] X.D. Wang, J.Z. Jiang, S. Yi, J. Non-Cryst. Solids **353**, 4157-4161 (2007).

[18] S.F. Guo, Z.Y. Wu, L. Liu, J. Alloys and Compd. **468**, 54-57 (2009).

[19] H.S. Chen, D. Turnbull, Acta Metallurgica **17**, 1021–1031 (1969).

[20] M.G. Nabiałek, M.J. Dośpiał, M. Szota, P. Pietrusiewicz, J. Jędryka, J. Alloys Compd, **509**, 3382–3386 (2011).

[21] S. Garus, M. Nabiałek, K. Błoch, J. Garus , Acta Physica Polonica, **126**, 957-959 (2014).

[22] G. Herzer, IEEE Trans. Magn., MAG-**26**, 1397 (1990).